

A comparative study of heat transfer characteristics of wall jet with boundary layer transition using six low-Reynolds number k - ϵ models

Cite as: AIP Advances 11, 025025 (2021); <https://doi.org/10.1063/5.0028978>

Submitted: 09 September 2020 . Accepted: 16 January 2021 . Published Online: 12 February 2021

 Xin Nie, Zehui Zhu, Haibo Liao, Ming Lü, and Jiangrong Xu

COLLECTIONS

Paper published as part of the special topic on [Chemical Physics](#), [Energy, Fluids and Plasmas](#), [Materials Science](#) and [Mathematical Physics](#)



View Online



Export Citation



CrossMark

ARTICLES YOU MAY BE INTERESTED IN

[Flow and thermal characteristics of three-dimensional turbulent wall jet](#)

Physics of Fluids **33**, 025108 (2021); <https://doi.org/10.1063/5.0031138>

[Bubble characteristics and turbulent dissipation rate in horizontal bubbly pipe flow](#)

AIP Advances **11**, 025125 (2021); <https://doi.org/10.1063/5.0035816>

[Label-free monitoring of immuno-specific interactions of adsorbed multilayer of proteins](#)

Biointerphases **16**, 011009 (2021); <https://doi.org/10.1116/6.0000669>



Call For Papers!

AIP Advances

SPECIAL TOPIC: Advances in Low Dimensional and 2D Materials

A comparative study of heat transfer characteristics of wall jet with boundary layer transition using six low-Reynolds number $k-\epsilon$ models

Cite as: AIP Advances 11, 025025 (2021); doi: 10.1063/5.0028978

Submitted: 9 September 2020 • Accepted: 16 January 2021 •

Published Online: 12 February 2021



View Online



Export Citation



CrossMark

Xin Nie,^{1,a)}  Zehui Zhu,¹ Haibo Liao,¹ Ming Lü,¹ and Jiangrong Xu²

AFFILIATIONS

¹School of Mechanical Engineering, Hangzhou Dianzi University, Hangzhou 310018, China

²School of Science, Hangzhou Dianzi University, Hangzhou 310018, China

^{a)}Author to whom correspondence should be addressed: nx2000@hdu.edu.cn. Tel.: +0086 13067984653

ABSTRACT

A Low-Reynolds Number (LRN) $k-\epsilon$ model can well simulate the transition characteristics of the momentum boundary layer, but so far, there are few studies on the influence of boundary layer transition on heat transfer characteristics by using the LRN $k-\epsilon$ model. Due to the larger degree of flexibility and controllability of flow parameters than the conventional boundary layer, a wall jet is an ideal flow configuration to research the transition of the boundary layer. To investigate the performance of the LRN $k-\epsilon$ model in simulating the heat transfer characteristics of the wall jet with boundary layer transition, six versions of LRN $k-\epsilon$ models are used to simulate a three-dimensional wall jet with boundary layer transition and the computational results were compared with experimental data. It is found that the Abe–Kondoh–Nagano (AKN) and Yang–Shih (YS) models can accurately simulate the flow field and heat transfer of the laminar boundary layer due to the use of the Kolmogorov scale in the developing region. Compared with the YS model, the AKN model is capable of predicting the influence of boundary layer transition on the heat transfer process in good agreement with experimental results over the whole domain. From the calculation results, it is found that Abid and Change and Hsieh and Chen models are more appropriate for simulating the heat transfer in the fully turbulent region of the wall jet. The damping function f_μ of the Lam–Bremhorst and Launder–Sharma models approaches a constant value near the wall, which does not meet the wall limiting conditions and leads to a negative impact on the simulation of heat transfer near the wall.

© 2021 Author(s). All article content, except where otherwise noted, is licensed under a Creative Commons Attribution (CC BY) license (<http://creativecommons.org/licenses/by/4.0/>). <https://doi.org/10.1063/5.0028978>

I. INTRODUCTION

A wall jet, formed by a high momentum fluid ejecting from a narrow slot along a flat plate, is a very common flow phenomenon and has been widely used in fluid heat transfer applications, such as electronic component cooling, defrosting and defogging of automotive windshield, and cooling of turbine vanes.^{1–3} It consists of two main parts: the inner shear layer near the wall similar to the wall boundary layer and the outer shear layer away from the wall.⁴ The development of the momentum boundary layer in the inner shear layer of the wall jet has a great influence on heat and mass transfer processes.⁵ Specifically, in the initial stage of the jet

development, during the transition from the laminar boundary layer to the turbulent boundary layer, the flow and heat transfer will change significantly.⁵ Earlier, Launder and Rodi⁶ have mentioned that the wall jet is an ideal flow configuration for resolving these intricate interactions that dominate the conventional turbulent boundary layer because it offers a larger degree of flexibility and controllability of parameters than a boundary layer does. Therefore, the research on the boundary layer flow field of the wall jet, especially the heat transfer characteristics of the thermal boundary layer, is still the focus of experimental and numerical research.

Abdulnour *et al.*⁷ summarized the previous experimental heat transfer studies^{8–10} on the wall jet and pointed out that

the measurement positions in these studies are all located in the range of $x/w > 30$, where the wall jet is in the fully turbulent region. However, combined with the motivation at that time, automotive defroster applications, the local heat transfer in the developing turbulent region ($0 < x/w < 13$) of the wall jet was more concerned. Hence, Abdulnour *et al.*⁷ measured the flow field and temperature field near the jet nozzle ($0 < x/w < 15$) using a hot wire anemometer, a microthermocouple, and infrared measuring devices. Furthermore, they provided the convection heat transfer coefficients and compiled the distribution of isothermal data points in the thermal boundary layer as shown in Fig. 1, which reflects an entire process of boundary layer transition of the wall jet. The work of Abdulnour *et al.*⁷ fills in the gaps of previous experiments and provides validation data for numerical simulations.

Over the past few years, previous researchers have carried out a lot of numerical simulation studies on the wall jet using turbulence models or the direct numerical simulation method.^{2,11–13} Among those turbulence models, the Low-Reynolds Number (LRN) $k-\epsilon$ models have been widely used to predict the wall jet due to their simplicity and capability of resolving the entire boundary layer including the viscous sublayer region near the wall. In the low-Reynolds number $k-\epsilon$ model, the damping function f_μ is used to make turbulent transport equations valid in the region of low Reynolds number near the wall so that the viscous sublayer near the wall can be directly solved. Compared with the $k-\epsilon$ model that uses the wall function to bridge the viscous and buffer layers, the low-Reynolds number $k-\epsilon$ model has theoretical advantages to the numerical simulation of the flow field and the heat transfer in the boundary layer.¹⁴ A review of transition predictions using four low-Reynolds number $k-\epsilon$ models has been provided by Abid.¹⁵ Abid¹⁵ concluded that the low-Reynolds number $k-\epsilon$ models are capable of predicting the qualitative aspects of transition and the start and end of transition were found to depend on the damp function f_μ .

In the past, the low-Reynolds number $k-\epsilon$ models have been widely used to simulate the flow physics of wall jets in the fully turbulent region and the boundary layer transition,^{11,13,15} but the capability of low-Reynolds number $k-\epsilon$ models to predict the heat

transfer characteristics of the wall jet with boundary layer transition has received little attention. In order to bridge this gap, the six low-Reynolds number $k-\epsilon$ models and the standard $k-\epsilon$ model with an enhanced wall function provided in the commercial computation fluid dynamics software FLUENT version 14.0 are used to carry out numerical simulations of the wall jets that were studied experimentally by Abdulnour *et al.*⁷ The simulated and experimentally measured transitional flow and heat transfer characteristics in the initial stage of the wall boundary layer were analyzed and evaluated in detail to provide a reliable reference for the selection of models in the field of low-Reynolds number wall jet research.

The six low-Reynolds number $k-\epsilon$ models tested were those developed by Launder and Sharma,¹⁶ Lam and Bremhorst,¹⁷ Abid,¹⁵ Yang and Shih,¹⁸ Abe, Kondoh and Nagano,¹⁹ and Change, Hsieh, and Chen,²⁰ respectively.

II. MATHEMATICAL MODEL

In the present study, it is assumed that the fluid (air) is essentially incompressible and Newtonian with temperature-dependent fluid properties. The wall jet flow is also assumed to be in a time-averaged quasi-steady state.

Therefore, the continuity equation is

$$\frac{\partial U_i}{\partial X_i} = 0, \tag{1}$$

and the Reynolds averaged Navier–Stokes equation is

$$U_i \frac{\partial U_j}{\partial x_i} = -\frac{1}{\rho} \frac{\partial P}{\partial x_i} + \frac{\partial}{\partial x_i} \left(\nu \frac{\partial U_i}{\partial x_j} - \overline{u_i u_j} \right). \tag{2}$$

The time-averaged energy equation is

$$U_i \frac{\partial T}{\partial x_i} = \frac{\partial}{\partial x_i} \left(\frac{\lambda}{c_p \rho} \frac{\partial T}{\partial x_j} - \overline{u_i t} \right). \tag{3}$$

In the above equation, the Reynolds stress terms are assumed to be proportional to the local mean velocity gradients through Boussinesq’s eddy transport approximation,

$$\overline{u_i u_j} = 2/3 k \delta_{ij} - \nu_t \left(\frac{\partial U_i}{\partial x_j} + \frac{\partial U_j}{\partial x_i} \right), \tag{4}$$

$$\overline{u_i t} = -\alpha_t \frac{\partial T}{\partial x_j}, \tag{5}$$

where the turbulent eddy viscosity and turbulent thermal diffusivity are given by

$$\nu_t = \frac{C_\mu f_\mu k^2}{\epsilon}, \tag{6}$$

$$\alpha_t = \frac{\nu_t}{\sigma_t}. \tag{7}$$

The transport equations for the $k-\epsilon$ model are

$$U_i \frac{\partial k}{\partial x_i} = \frac{\partial}{\partial x_j} \left[\left(\nu + \frac{\nu_t}{\sigma_k} \right) \frac{\partial k}{\partial x_j} \right] + P_k - \epsilon - D, \tag{8}$$

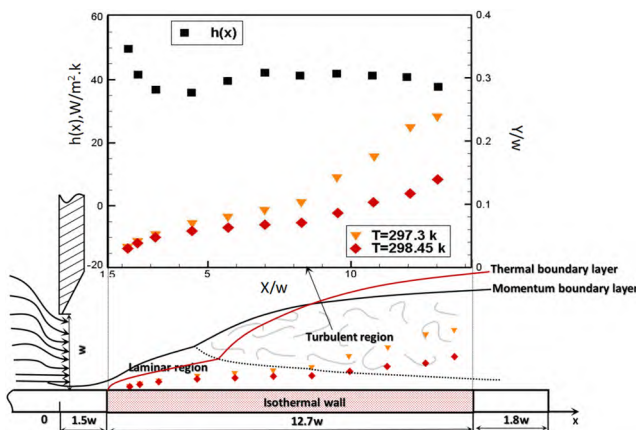


FIG. 1. Schematic configuration of the wall jet.

TABLE I. Summary of model constants and D and E terms in governing equations.

Model	D	E	Wall BC	C_μ	C_1	C_2	σ_k	σ_ε
SKE	0	0	Wall functions	0.09	1.44	1.92	1	1.3
AB	0	0	$\varepsilon_w = \nu \left(\frac{\partial^2 k}{\partial y^2} \right)$	0.09	1.45	1.83	1	1.4
LB	0	0	$\varepsilon_w = \nu \left(\frac{\partial^2 k}{\partial y^2} \right)$	0.09	1.44	1.92	1	1.3
LS	$2\nu \left(\frac{\partial \sqrt{k}}{\partial y} \right)^2$	$2\nu v_t \left(\frac{\partial^2 U}{\partial y^2} \right)^2$	$\tilde{\varepsilon}_w = 0$	0.09	1.44	1.92	1	1.3
YS	0	$\nu v_t \left(\frac{\partial^2 U}{\partial y^2} \right)^2$	$\varepsilon_w = \nu \left(\frac{\partial^2 k}{\partial y^2} \right)$	0.09	1.44	1.92	1	1.3
AKN	0	0	$\varepsilon_w = \nu \left(\frac{\partial \sqrt{k}}{\partial y} \right)^2$	0.09	1.44	1.9	1.4	1.4
CHC	0	0	$\varepsilon_w = \nu \left(\frac{\partial^2 k}{\partial y^2} \right)$	0.09	1.44	1.92	1	1.3

$$U_i \frac{\partial \tilde{\varepsilon}}{\partial x_i} = \frac{\partial}{\partial x_j} \left[\left(\nu + \frac{v_t}{\sigma_\varepsilon} \right) \frac{\partial \tilde{\varepsilon}}{\partial x_j} \right] + C_{\varepsilon 1} f_1 \frac{1}{T_t} P_k - C_{\varepsilon 2} f_2 \frac{\tilde{\varepsilon}}{T_t} + E, \quad (9)$$

where \bar{u}_i is the fluctuation velocity, \bar{t} is the fluctuation temperature, and the model parameters f_μ , f_1 , f_2 , $\tilde{\varepsilon}$, D , and E vary with the different models; f_μ , f_1 , and f_2 are the damping functions of the local turbulent Reynolds number, $\tilde{\varepsilon}$ is the modified isotropic dissipation rate related to ε , D and E are additional source items, and P_k is the turbulent kinetic energy production term. In the low-Reynolds number k - ε model, the turbulent eddy viscosity coefficient is defined by Eq. (6), where C_μ is a constant and f_μ is a damping function. The turbulent thermal diffusivity coefficient α_t is obtained using Eq. (7) with turbulent Prandtl number σ_t . The Prandtl number and turbulent Prandtl number are taken to be 0.71 and 0.9 for air,²¹ respectively. T_t in Eq. (9) is the turbulence timescale expressed as k/ε .

The low-Reynolds number region is characterized by the direct effect of molecular viscosity on turbulent momentum. When the turbulent Reynolds number Re_t is less than 150, the effect of molecular viscosity is more significant, commonly known as low-Reynolds number flow. The following is a brief introduction to the six low-Reynolds number k - ε models used in this paper:

Launder and Sharma model¹⁶ (hereafter referred to as LS): The LS model, which uses Re_t (defined as k^2/ε) to construct the functions f_μ and f_2 , was first proposed by Jones and Launder and modified by Launder and Sharma. Due to the advantages of zero Neumann boundary condition²² and in order to obtain a satisfactory distribution of turbulent kinetic energy near the wall, the additional terms D and E are added in the turbulent kinetic energy and dissipation equation.

Lam and Bremhorst model¹⁷ (hereafter referred to as LB): The LB model uses Re_t and Re_y (defined as $\nu k^{0.5}/\nu$) to construct the functions, f_μ , f_1 , and f_2 and does not include additional terms in the k and ε equation. This model was proved to be valid through the fully turbulent, semilaminar, and laminar regions of the flow by application to fully development pipe flow.

Abid model¹⁵ (hereafter referred to as AB model): The AB model was designed for forecasting the process of transition from the laminar to turbulent flow and showed a good capability for predicting bypass transition on a flat plate.

Yang and Shih model¹⁸ (hereafter referred to as YS model): The YS model was proposed to accurately capture the near-wall flows in the wall bound turbulent boundary layer. In this model, the Kolmogorov timescale is added to turbulent timescale, which ensures that there is no singularity at the wall, and the introduction of a pseudo-dissipation rate is avoided. Hence, the timescale of the YS model can be expressed as follows:

$$T_t = k/\varepsilon + C_k(\nu/\varepsilon)^{1/2},$$

where C_k is the Kolmogorov constant and taken to be 1.

Abe, Kondoh, and Nagano¹⁹ model (hereafter referred to as AKN model): The AKN model is a modified version of the low-Reynolds number two-equation heat-transfer model proposed by Nagano *et al.*, in which the main improvement is to replace friction velocity u_τ with the Kolmogorov velocity scale $u_\varepsilon = (\nu\varepsilon)^{1/4}$ so that the AKN model can account for the near-wall and low-Reynolds number effects in both attached and detached flows.

Change, Hsieh, and Chen²⁰ model (hereafter referred to as CHC model): The CHC model is capable of correctly predicting the near-wall limiting flow behavior while avoiding occurrence of the singular difficulty near the reattachment point as applying to the recirculating flow in sudden-expansion pipe.

The damping functions f_μ , f_1 , and f_2 are varied with different low-Reynolds number k - ε models (see Table II for details). It is noted that the friction velocity u_τ is not included in the damping function definition of the above six low-Reynolds number models, and so those models can be used for the flow with boundary transition separation. The relevant model constants $C_{\varepsilon 1}$, $C_{\varepsilon 2}$, C_μ , σ_k , and σ_ε in some of the models are also modified, which are different from the standard k - ε model (see Table I for details).

III. PROBLEM DESCRIPTION

A. Simulation details and boundary conditions

The schematic diagram of the numerical simulation domain of the wall jet is shown in Fig. 1. The grid divisions and boundary conditions were consistent with experiments,⁷ with the following specific settings: the nozzle width was $w = 20$ mm; the nozzle throat thickness in the X direction was 19 mm; the horizontal length of the bottom wall was $x = 16w$; the bottom wall was divided into three

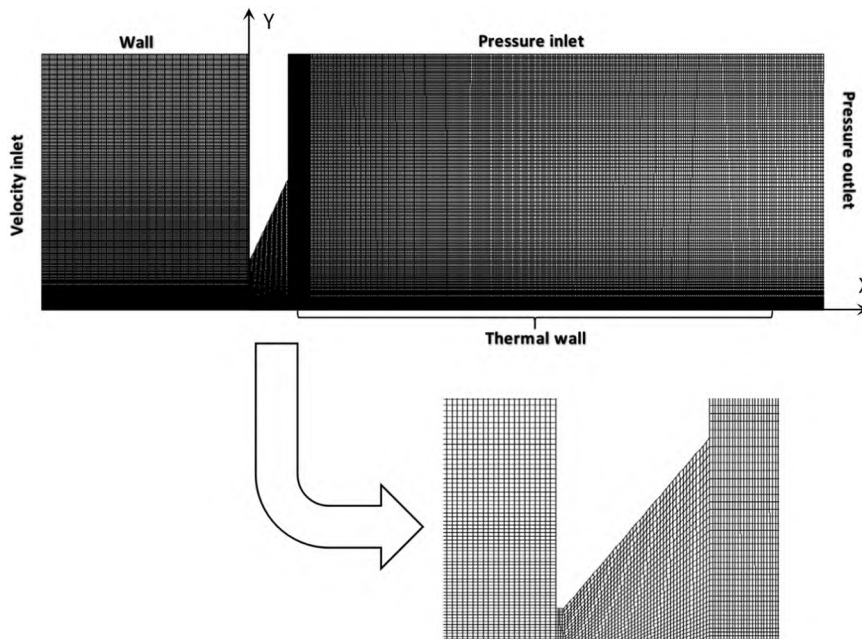


FIG. 2. Grid distribution for the jet slot.

parts: $0 \leq x_1 < 1.5w$ part was specified as an adiabatic wall; the wall section $1.5w \leq x_2 < 14.2w$ part was specified as an isothermal wall, and the temperature is 45°C ; and the wall section $x_3 \geq 14.2w$ part was specified as an adiabatic wall. The vertical height of the domain is $Y = 5w$, and the jet temperature is the same as room temperature set at 22°C ; therefore, select the air properties of 22°C . The inlet Reynolds number is 7700, where the characteristic length was the nozzle width set as 0.02 m and the characteristic velocity was the average inlet velocity U_0 set as 6.1 m/s. Meanwhile, the turbulence intensity and length scale at the nozzle exit were set to be 5% and $0.07w$, respectively. Hence, the initial value k at the nozzle exit was calculated from $k = 1.5 \cdot (I \cdot U)^2$ and the initial value ϵ was calculated from $\epsilon = (k^{3/2} \cdot C_\mu^{3/4}) / 0.07w$. The boundary condition for turbulent kinetic energy is $k = 0$ at the solid wall. But the specific boundary

condition for the turbulent dissipation rate at the solid wall is varied with different low-Reynolds number $k-\epsilon$ models (see Table I for details).

B. Numerical scheme and grid independence study

In the present work, the semi-implicit method for pressure-linked equations (SIMPLE) is followed to handle the velocity and pressure coupling. The power-law upwind and second-order central-difference schemes are used to discretize the convective and diffusive terms, respectively.¹¹ The convergence criteria are specified as follows: the normalized residuals of all dependent variables must be less than 10^{-6} . After reaching the criteria, we set the residual value to 10^{-7} and calculate 5000 steps of iteration again. Comparing

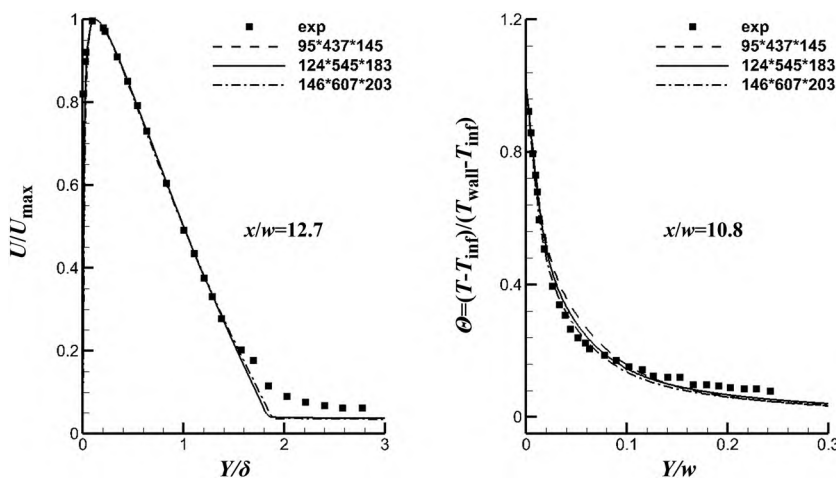


FIG. 3. Grid independence study.

the temperature and flow field at $x/w = 10.8$ and $x/w = 12.7$, when the maximum difference between the results is not more than 0.1%, it can be considered that the calculation has converged. The convergence results of $k-\epsilon$ models are used as the initial field for all low-Reynolds number models. Figure 2 shows the entire and local view of grid distribution for the jet slot.

To resolve the near wall region with large gradients satisfactorily, finer computational grids were set near the wall and the distance of the first grid near the wall Y_{plus} was taken as a different value in different literature studies.^{11,13,21} In this paper, we set up three to five grid layers in the bottom layer ($Y_{plus} < 5$) of viscous laminar flow near the wall to ensure that the first near-wall grid points lie in the viscous sublayer for low-Reynolds number $k-\epsilon$ models.

For all experiment conditions and models, the grid independence study has been carried out for the wall jet at three grid sizes, viz., $95 \times 437 \times 145$ (6 019 675), $124 \times 545 \times 183$ (12 367 140), and $146 \times 607 \times 203$ (17 990 266). As shown in Fig. 3, the velocity distribution of the flow field and the temperature distribution of the whole thermal boundary calculated by the AKN model¹⁹ in the self-similar region $x/w = 12.7$ and $x/w = 10.8$ were compared with the experimental data, respectively, and it can be seen that the calculation results of three sizes of grids have a good consistency.

Y_{plus} is the distance normal to the wall in the outer layer (where $u/u_m = 0.5$) and was used for the dimensionless distance in the Y direction; θ is the dimensionless temperature, T_{inf} is the jet temperature, and T_{wall} is the wall temperature. When the computing

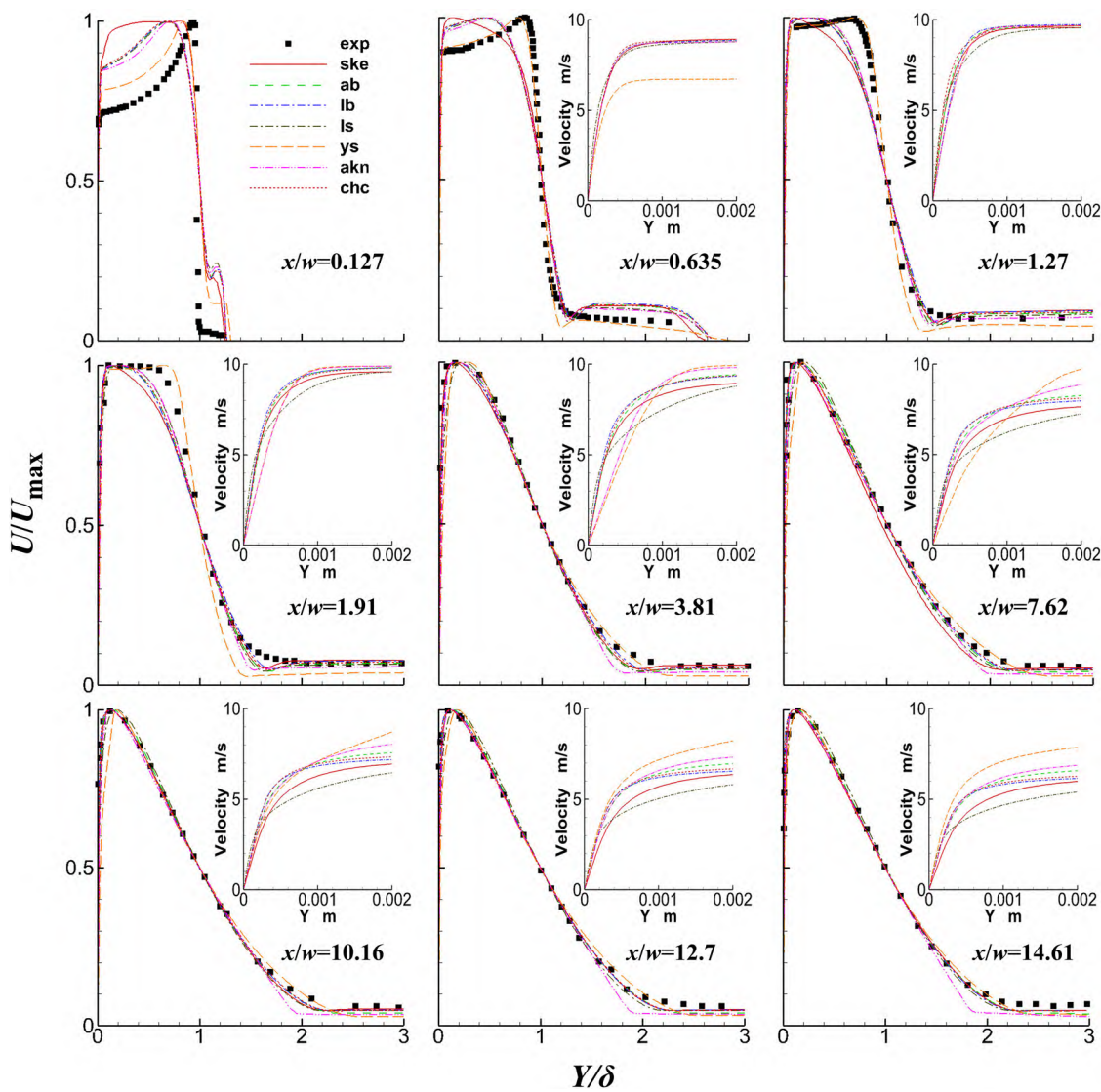


FIG. 4. Comparison of the velocity profile with experimental data.

resources are allowed, the dense node distribution of the grid should be selected as much as possible. Considering the available computing resources and the cycle of numerical simulation, the grid size of $124 \times 545 \times 183$ (12 367 140) is considered for simulation finally.

IV. RESULTS AND DISCUSSION

A. Discussion on the flow field and developing boundary layer characteristics of the wall jet

Figure 4 shows a comparison of dimensionless velocity profiles for the wall jet at different streamwise positions predicted by six low-Reynolds number k - ϵ models with experimental data. The upper right corner is a locally enlarged view of the absolute velocity field near the wall.

It is seen from Fig. 4 that most of the models tested capture the shape of the dimensionless velocity profile in the self-similar region ($x/w > 7.62$) quite well but have some difference with experimental data in the developing region ($0.127 \leq x/w \leq 3.81$).

In the wall jet developing region, there exists a great velocity gradient near the wall, which leads to a higher viscous shear stress and a thinner laminar boundary layer. It can be verified from the streamwise rms intensity distribution near the nozzle measured by Abdunour *et al.*⁷ Due to the strong three-dimensional nonlinear effect of the flow field near the nozzle, the linear eddy viscosity turbulence model based on Boussinesq hypothesis has some deviations.²³ It is noted that the YS model shows very good agreement with experimental data in the developing region. For most turbulence models used in this paper, the definition of the modified damping function f_1 of the production term in the dissipation equation is equal to 1 (see Table II for details). Instead, the modified damping function f_1 in the YS model is expressed as $f_1 = 1/\text{Re}_t^{0.5} + 1$, which makes up for the deficiency of Boussinesq's linear eddy viscosity hypothesis to some extent.²³

Abdunour *et al.*⁷ pointed out that a self-preserving form of the jet was established for $x/w \geq 6.9$, which means that the wall jet enters the self-similar region and the dimensionless velocity profile does not change with the streamwise distance. In the self-similar region, the wall jet gradually enters the stage of fully turbulent development, which can also be confirmed by the measurement results of streamwise rms intensity distribution in the self-similar region in the study by Abdunour *et al.*⁷ With the development of the turbulent wall jet, the dimensionless velocity profile predicted by all turbulence models gets closer to experimental data. Among those models, the computational results obtained from the AB model, CHC model, and the standard k - ϵ model using the enhanced wall function are in excellent agreement with the experimental data in the self-similar region.

As important turbulent scalars describing the state of the boundary layer,²⁴ it is necessary to combine the turbulent kinetic energy and dissipation rate to further discuss the capabilities of six low-Reynolds number k - ϵ models for predicting the developing boundary layer characteristics of the wall jet. Figures 5 and 6 show turbulent kinetic energy and dissipation rate profiles for the wall jet at different streamwise positions predicted by six low-Reynolds number k - ϵ models. The upper right or left corner is a locally enlarged view of the turbulent kinetic energy and dissipation rate profile near the wall.

It is seen from Figs. 5 and 6 that the turbulent kinetic energy and dissipation rate profiles predicted by all low-Reynolds number k - ϵ models have two extremes when the streamwise distance is $x/w \geq 3.18$, where the transition from laminar to turbulent flow has already begun in the boundary layer. One extreme is located in the outer shear layer far away from the wall, and the velocity reaches a maximum here; the other located in the inner shear layer near the wall is caused by the burst of turbulent vortices near the viscous bottom.¹⁴

TABLE II. Summary of damping functions appearing in the governing equations.

Model	f_μ	f_1	f_2
SKE	1.0	1.0	1.0
AB	$\tanh(0.008\text{Re}_y) \times (1 + 4/\text{Re}_t^{0.75})$	1.0	$1 - 2\{\exp(-\text{Re}_t^2/36) \cdot [1 - \exp(-\text{Re}_y/12)]\}/9$
LB	$(1 - \exp(-0.0165\text{Re}_y))^2 \times (1 + 20.5/\text{Re}_t)$	$1 + (0.005/f_\mu)^3$	$1 - \exp(-\text{Re}_t^2)$
LS	$\exp[-3.4/(1 + \text{Re}_t/50)^2] \cdot (1 + 1/\text{Re}_t^{0.5})[1 - \exp(-1.5 \times 10^{-4} \cdot \text{Re}_y - 5 \times 10^{-7} \text{Re}_y^3 - 10^{-10} \text{Re}_y^5)]^{0.5} (1 + \text{Re}_t^{0.5})$	$\text{Re}_t^{0.5}/(1 + \text{Re}_t^{0.5})$	$\text{Re}_t^{0.5}/(1 + \text{Re}_t^{0.5})$
YS	$\{1 + (5/\text{Re}_t^{0.75}) \exp[-(\text{Re}_t/200)^2]\} \cdot [1 - \exp(-y^*/14)]^2$	1.0	$\{1 - 0.3 \exp[-(\text{Re}_t/6.5)^2]\} \cdot [1 - \exp(-y^*/3.1)]^2$
AKN	$[1 - \exp(-0.0215\text{Re}_y)]^2 \cdot (1 + 31.66/\text{Re}_y^{1.25})$	1.0	$[1 - 0.01 \exp(-\text{Re}_t^2)] \cdot [1 - \exp(-0.0631\text{Re}_y)]$
CHC			

When the streamwise distance is located in $0.127 \leq x/w \leq 3.81$, the state of the boundary layer in the inner shear layer is almost laminar, which can also be verified from the streamwise rms intensity distribution measured by Abdunour *et al.*⁷ The turbulent kinetic energy and dissipation rate profile near the wall predicted by most low-Reynolds number $k-\varepsilon$ models show an extreme value since $x/w \geq 1.27$ and lead to a premature estimation of boundary layer transition. Instead, the prediction results of the YS model and the AKN model do not show obvious extreme values but approximate to zero, which is consistent with the flow characteristics of the laminar boundary layer. The better capabilities of YS and AKN models for predicting boundary layer transition in the wall jet may be due to the use of the Kolmogorov scale.

Diez *et al.*²⁵ mentioned that the Kolmogorov scale arguably represents the smallest scales in the flow where viscous dissipation dominates and where the energy cascade ends. Rathore and Das^{11,13,21} have reported the advantage of the YS model using the Kolmogorov timescale in predicting the turbulent kinetic energy near the wall many times. On the other hand, Masahide Inagaki²⁶ reported the effectiveness of the improved wall-damping function by using the Kolmogorov velocity scale instead of friction velocity in the Reynolds Averaged Navier-Stokes equations (RANS) model and tried to employ this wall-damping function in large eddy simulation (LES).

In the meantime, it is noted that the velocity gradient near the wall predicted by YS and AKN models is almost coincident and

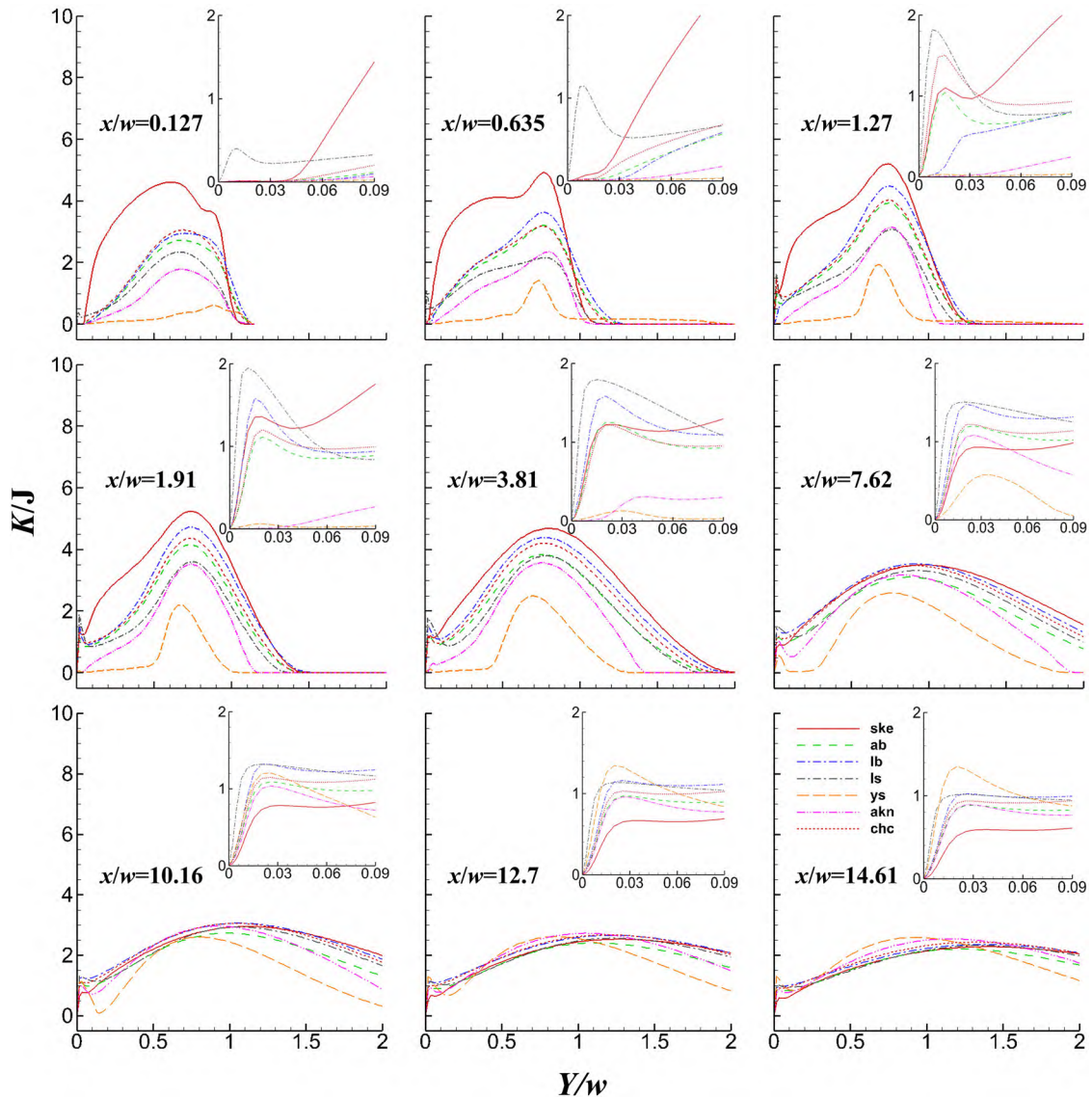


FIG. 5. Calculation results of turbulent kinetic energy of the wall jet.

bigger than that predicted by other low-Reynolds number $k-\epsilon$ models at the streamwise distance of $1.27 \leq x/w \leq 3.81$, which further shows the flow characteristic of the laminar boundary layer (see the locally enlarged view in Fig. 4 for details). However, the turbulent kinetic energy and dissipation rate near the wall predicted by the YS model are relatively small in the wall jet developing region so that the decay of the jet gets slower and the laminar boundary layer region gets longer and thicker, which leads to the transition to the turbulent boundary layer slower (see the locally enlarged view in Figs. 4–6 for details).

The turbulent dissipation rate ϵ predicted by the LS model has an abnormally large extremum near the wall, which may lead to faster decay than other low-Reynolds number $k-\epsilon$ models and an adverse effect on calculation results (see the locally enlarged view in

Figs. 4 and 6 for details). Similar problems are also mentioned in the literature.^{14,27}

B. Discussion on the calculation results of the temperature field near the wall and the heat transfer process

Figure 7 shows the dimensionless temperature profiles in the entire thermal boundary layer. The upper left corner shows the dimensionless temperature profiles in the thermal sublayer.

It is well-known that velocity and temperature vary linearly in the viscous and thermal sublayer. Compared with other low-Reynolds number $k-\epsilon$ models, YS and AKN models can predict an

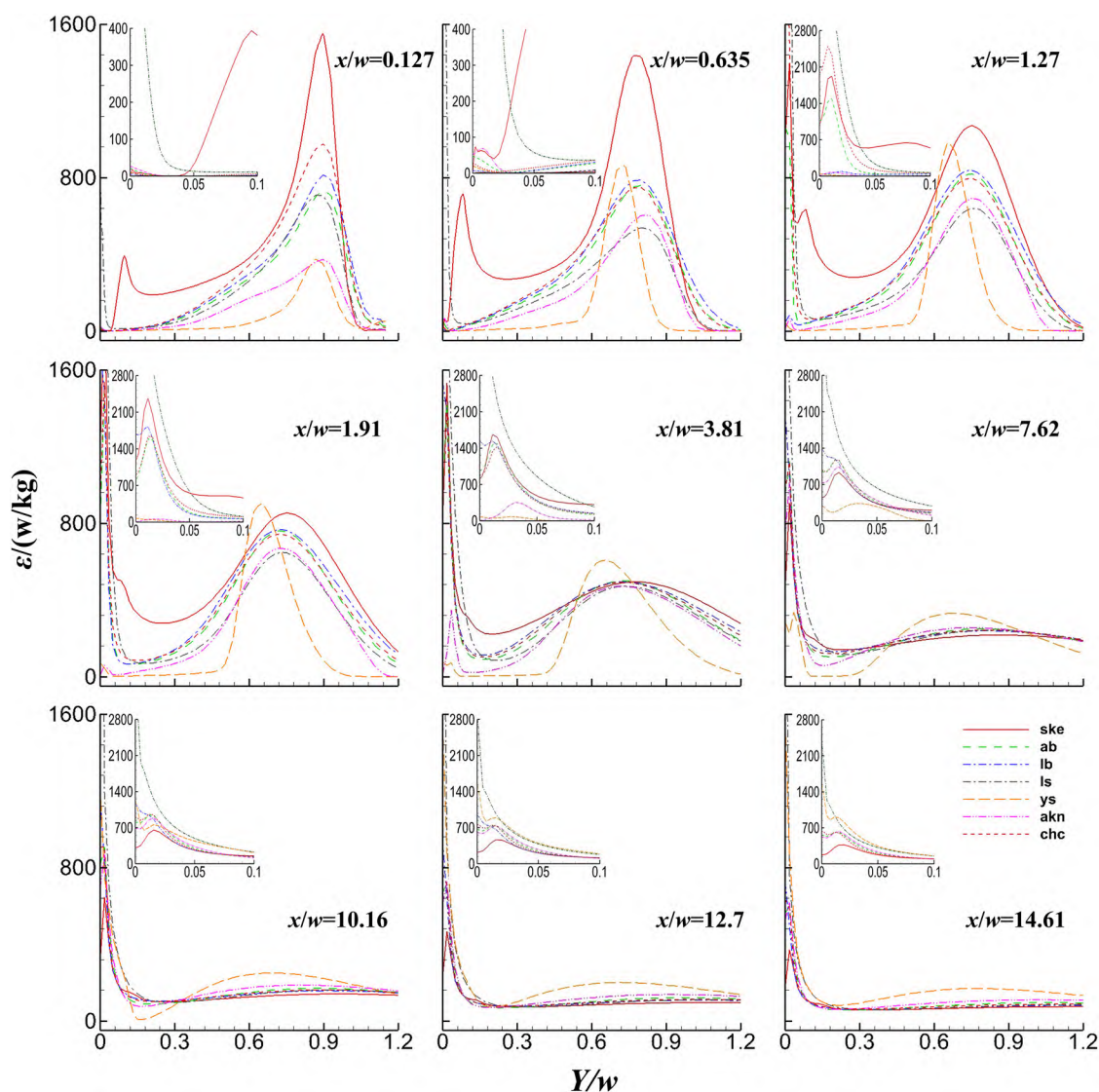


FIG. 6. Calculation results of the turbulent dissipation rate of the wall jet.

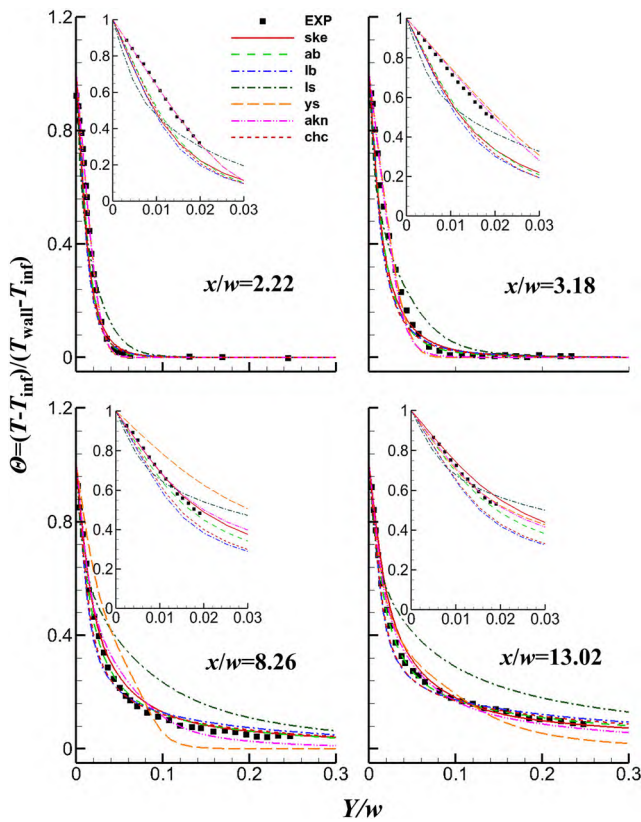


FIG. 7. Comparison of non-dimensional near-wall temperature profiles in and throughout the thermal boundary layer with experimental data.

obvious linear decay of temperature in the thermal sublayer and have an excellent agreement with experimental data (see the locally enlarged view in Fig. 7 for details). Meanwhile, it is interesting to note that the dimensionless temperature profiles predicted by YS and AKN models are almost coincident at streamwise distances of $x/w = 2.22$ and $x/w = 3.18$ just like the velocity gradient near the wall at streamwise distances of $1.27 \leq x/w \leq 3.81$ (see the locally enlarged view in Fig. 4 for details). In heat transfer modeling, for six low-Reynolds number $k-\epsilon$ models, the turbulent thermal diffusivity coefficient a_t is obtained using Eq. (7) with turbulent Prandtl number σ_t .

Sommer *et al.*²⁸ mentioned that in incompressible non-buoyant flows, turbulent heat fluxes were directly determined from turbulent momentum fluxes, which further argued that the prediction results of velocity near the wall have a significant impact on heat transfer. Due to a relatively longer and thicker laminar boundary layer region, the YS model underestimated the thermal diffusivity between fluids, which leads to an obvious difference between the dimensionless temperature profiles predicted by the YS model and experimental data at a streamwise distance of $x/w = 8.26$ (see the locally enlarged view in Fig. 7 for details). In the meantime, the dimensionless temperature profiles obtained from the AB model, CHC model, and the standard $k-\epsilon$ model using the enhanced wall function get closer to experimental data at streamwise distances of $x/w = 8.26$ and x/w

$= 13.02$ just like dimensionless velocity profiles in the similar region of the wall jet. Due to the abnormally large turbulent dissipation rate ϵ near the wall, the turbulent eddy viscosity calculated by the LS model will become smaller and, furthermore, the turbulent thermal diffusivity gets smaller near the wall, which leads to the dimensionless temperature profiles predicted by the LS model that show an obvious nonlinear distribution (see the locally enlarged view in Fig. 7 for details). Among those models, the AKN model shows an excellent agreement with experimental data in the thermal boundary layer whether the wall jet is in the developing region or self-similar region.

In order to further investigate the capabilities of low-Reynolds number $k-\epsilon$ models for predicting the influence of boundary layer transition on the entire heat transfer process, this paper gives a comparison of the convection heat transfer coefficient h_x with experimental data as shown in Fig. 8. h_x was calculated from the following expression:

$$h(x) = \frac{-\lambda(\partial T/\partial y)_{y \rightarrow 0}}{(T_{wall} - T_{jet})},$$

where T_{wall} is the wall temperature, T_{jet} is the jet temperature, and λ is the thermal conductivity.

According to the experimental data, the heat transfer coefficient is very high near the nozzle exit due to higher jet momentum. The jet momentum decreases downstream due to the exchange of momentum with the surrounding fluid. Subsequently, the heat transfer coefficient begins to rise due to boundary layer transition and tends to be flat. At the streamwise distance of $0 \leq x/w \leq 3.81$, YS and AKN models capture the shape of h_x quite well due to the accurate calculation results of the temperature gradient in the thermal sublayer. It is noted that the heat transfer coefficient begins to rise around $x/w = 4$ from experimental data, which means that the boundary layer is transitioning from laminar to turbulent flow. The AKN model can accurately capture the location of transition and have a good agreement with experimental data.

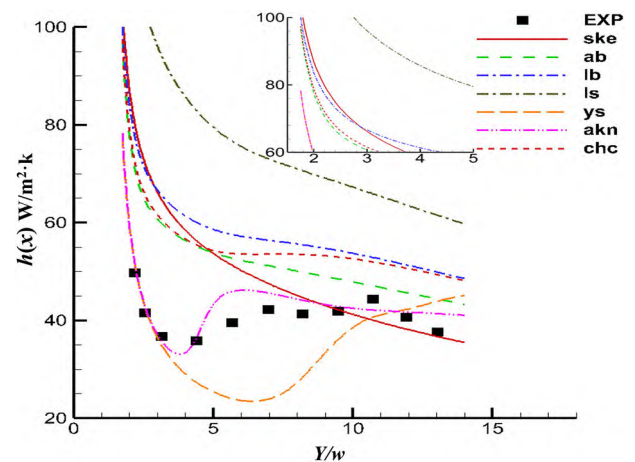


FIG. 8. Comparison of the convection heat transfer coefficient with experimental data.

On the contrary, as previously mentioned, the YS model overestimated the development of the laminar boundary layer due to the relatively small turbulent kinetic energy and dissipation rate in the wall jet developing region, which leads to a smaller heat transfer coefficient and a relatively backward location of transition around $x/w = 6.3$.

Except for the YS and AKN model, the other models overestimated the magnitudes of h_x due to the excessive temperature gradient in the thermal sublayer and almost cannot predict the influence of boundary layer transition on heat transfer. Abid mentioned that the position of boundary layer transition predicted by low-Reynolds number k - ε models depends on the damp function f_μ .¹⁵ Petal *et al.*²⁹ summarized the previous low-Reynolds number k - ε models, and based on the theory of dimensional analysis, they pointed out that the limiting conditions of near wall turbulence have the following relations: when $y \rightarrow 0$, $-\overline{u'v'} \propto y^3$, $k \propto y^2$, $\nu_t \propto y^3$, $\varepsilon \rightarrow \varepsilon_w$, and $f_\mu \rightarrow y^{-1}$. According to the formula in Table I, when the distance from the wall is close to 0, the most critical damping functions f_μ of different low-Reynolds number k - ε models have different characteristics. For AB, AKN, CHC, and YS models, $f_\mu \rightarrow y^{-1}$ meets the wall limiting conditions. However, for LB and LS models, $f_\mu \rightarrow \text{constant}$ does not meet the wall limiting conditions, which may lead to the smaller turbulent viscosity ν_t calculated by LB and LS models [see formula (6)] and further cause smaller α_t [see formula (7)]. As previously mentioned, the relatively small turbulent thermal diffusivity calculated by the LS model due to the abnormally large turbulent dissipation rate ε near the wall also leads to an obvious larger heat transfer coefficient than experimental data. To a large extent, the calculation results of different low-Reynolds number k - ε models are influenced by these damping functions, source terms, and constant coefficient of models in the transport equation.

Obviously, except the AKN model, the other five low-Reynolds number k - ε models fail to predict the influence of boundary layer transition on the entire heat transfer process.

V. CONCLUSION

A comparative study of heat transfer characteristics of the wall jet with boundary layer transition was carried out using six low-Reynolds number k - ε models. The calculation results were compared with the available experimental data. Some of the specific conclusions are summarized as follows:

- In the wall jet developing region, AKN and YS models can accurately simulate the flow field and heat transfer of the laminar boundary layer due to the use of the Kolmogorov scale.
- The YS model can capture the shape of the dimensionless velocity profile quite well near the nozzle exit in the developing region due to the modified damping function f_1 . However, the position of boundary layer transition predicted by the YS model is relatively backward, which leads to a longer and thicker laminar boundary layer region and a small heat transfer coefficient.
- Regarding the relative performance of various low-Reynolds number k - ε models tested, the AKN model is capable of predicting the influence of boundary layer transition on

the heat transfer process in good agreement with experimental results over the whole domain.

- Although AB and CHC models fail to simulate the influence of boundary layer transition on the heat transfer process, the flow and temperature field predicted by AB and CHC models in the self-similar region have a good agreement with experimental data, which means that AB and CHC models are more appropriate for simulating the heat transfer in the fully turbulent region of the wall jet.
- The damping function f_μ in the LB and LS models does not meet the wall limiting conditions, which leads to a negative impact on the simulation of heat transfer near the wall. The abnormally large turbulent dissipation rate ε near the wall leads to a bigger deviation between the LS model and experimental data.

NOMENCLATURE

$C_{\varepsilon 1}$, $C_{\varepsilon 2}$, and C_μ	turbulence model constants
C_p	specific heat
D and E	additional source items
f_μ , f_1 , and f_2	damping functions
h	surface heat transfer coefficient
I	turbulence intensity
k	turbulent kinetic energy
P	static pressure
P_k	turbulent kinetic energy production term
T	temperature
T_t	turbulence timescale
\bar{t}	fluctuation temperature
U	time-averaged velocity
\bar{u}_i	fluctuation velocity
x, y	coordinates
Y_{plus}	dimensionless distance $Y_{plus} = u_\tau y \rho / \mu$
$\tilde{\varepsilon}$	modified isotropic dissipation rate related to ε
w	nozzle width

Greek symbols

μ and μ_t	Laminar and eddy viscosities
ν and ν_t	Laminar and eddy kinematic viscosities
α	thermal conductivity
α_t	turbulent thermal diffusivity
ρ	density
ε	turbulent dissipation rate
σ_k , σ_ε , and σ_t	turbulent Prandtl numbers

Dimensionless group

Re	jet Reynolds number based on jet inlet velocity and hydraulic diameter, $Re = \rho u_j w / \mu_t$
Re_T and Re_y	turbulence Reynolds numbers
δ	the distance normal to the wall in the outer layer

Subscripts

T_{inf}	jet temperature
T_{wall}	wall temperature

DATA AVAILABILITY

The data that support the findings of this study are available from the corresponding author upon reasonable request.

REFERENCES

- ¹W.-x. Huai, Z.-w. Li, Z.-d. Qian, Y.-h. Zeng, J. Han, and W.-q. Peng, *J. Hydrodyn.* **22**(1), 58–65 (2010).
- ²T. P. Singh, A. Kumar, and A. Satapathy, *Numer. Heat Transfer, Part A* **77**(2), 179–198 (2020).
- ³K. K. Mohseni, *Eur. J. Mech. B: Fluid* **29**(4), 269–277 (2010).
- ⁴S. Bhatt, S. Artham, R. Mankbadi, and E. Gnanamanickam, in APS Meeting, 2014.
- ⁵F. B. Hsiao and S. S. Sheu, *Aeronaut. J.* **100**(999), 373–380 (2016).
- ⁶B. E. Launder and W. Rodi, *Annu. Rev. Fluid Mech.* **15**(1), 429–459 (1983).
- ⁷R. S. AbdulNour, K. Willenborg, J. J. McGrath, J. F. Foss, and B. S. AbdulNoura, *Exp. Therm. Fluid Sci.* **22**(3), 123–131 (2000).
- ⁸I. Mabuchi and M. Kumada, *Trans. Jpn. Soc. Mech. Eng.* **88**(15), 1236–1245 (1972).
- ⁹J. C. Akfirat, in Proceedings of the Third International Heat Transfer Conference, 1966.
- ¹⁰P. Y. Nizou and T. Tida, *Int. J. Heat Mass Transfer* **7**(38), 1187–1200 (1995).
- ¹¹S. K. Rathore and M. K. Das, *Int. J. Heat Mass Tran.* **61**(6), 365–380 (2013).
- ¹²I. Z. Naqavi, J. C. Tyacke, and P. G. Tucker, *Int. J. Heat Fluid Flow* **63**(2), 99–107 (2016).
- ¹³S. K. Rathore and M. K. Das, *Int. J. Therm. Sci.* **89**, 337–356 (2015).
- ¹⁴X. Nie, Y. Zhang, T. Zhang, L. Li, and J. Xu, *Proc. CSEE* **37**(024), 7247–7254 (2017).
- ¹⁵R. Abid, *Int. J. Eng. Sci.* **31**(6), 831–840 (1993).
- ¹⁶B. E. Launder and B. I. Sharma, “Application of the energy-dissipation model of turbulence to the calculation of flow near a spinning disc,” *Lett. Heat Mass Transfer* **1**(2), 131–138 (1974).
- ¹⁷C. Lam and K. Bremhorst, *J. Fluid Eng. T. ASME* **103**(1), 183–205 (1991).
- ¹⁸Z. Yang and T. H. Shih, *AIAA J.* **31**(7), 1191–1198 (1993).
- ¹⁹K. Abe, T. Kondoh, and Y. Nagano, *Int. J. Heat Mass Transfer* **37**(1), 139–151 (1994).
- ²⁰C. K. Change, W. D. Hsieh, and C. S. Chen, *J. Fluid Eng.* **3**(117), 417–423 (1995).
- ²¹S. K. Rathore and M. K. Das, *Int. J. Heat Mass Transfer* **95**(5), 636–649 (2016).
- ²²W. P. Jones and B. E. Launder, *Int. J. Heat Mass Transfer* **15**(2), 301–314 (1972).
- ²³L. Zhang, J. Zhou, and X. Chen, *J. Cent. South Univ. Technol.* **04**(8), 564–568 (2008).
- ²⁴V. Michelassi, W. Rodi, and J. Zhu, *AIAA J.* **31**(9), 1720–1723 (2012).
- ²⁵F. J. Diez, Y. Cheng, and A. Villegas, *Exp. Therm. Fluid Sci.* **35**(6), 1223–1229 (2011).
- ²⁶M. Inagaki, *Int. J. Heat Fluid Flow* **32**(1), 26–40 (2011).
- ²⁷A. Mathur and S. He, *Comput. Fluids* **79**(6), 134–139 (2013).
- ²⁸Y. G. and R. M. C. S. Lai, *Int. J. Heat Mass Transfer* **12**(35), 3375–3387 (1992).
- ²⁹V. C. Patel, W. Rodi, and G. G. Scheuerer, *AIAA J.* **23**(9), 1308–1319 (1985).